(Received 16 September 2025, Accepted 13 November 2025, Scheduled 19 November 2025)

Adaptive Non-Singular Terminal Sliding Mode Control of PMSM Based on Nonsingular Fast Terminal Double Power Sliding Mode Disturbance Observer

Junqin Liu[1,*], Zhentong Wang[1], Tianle Li[1], Feng Deng[1], Xinchun Jiang[2], Kaihui Zhao[2], and Xiangfei Li[2]

[1] *National Key Laboratory of Power Grid Disaster Prevention and Mitigation (College of Electrical and Information Engineering Changsha University of Science and Technology), Changsha, Hunan 410114, China*
[2] *College of Transportation and Electrical Engineering, Hunan University of Technology, Zhuzhou 412007, China*

ABSTRACT: This paper proposes a composite control strategy integrating Adaptive Non-singular Terminal Sliding Mode Control (ANTSMC) with a Non-singular Fast Terminal Double-Power Sliding Mode Observer (NFTDPSMO) to achieve the high-precision control of PMSM system. The strategy combines an adaptive non-singular terminal sliding mode controller with a novel sliding mode disturbance observer. The ANTSMC adaptively adjusts the convergence speed according to the distance between the system state and sliding surface to suppress chattering, while the NFTDPSMO employs a triple-composite term with denominator modification to achieve singularity-free operation and global fast convergence. Simulated and experimental results demonstrate that under complex operating conditions including parameter perturbations, load variations, and external disturbances, the proposed composite controller achieves faster dynamic response, reduced current and torque pulsations, lower harmonic distortion (THD of only 7.1%), and significantly enhanced robustness and steady-state performance.

1. INTRODUCTION

Permanent Magnet Synchronous Motors (PMSMs) have attracted considerable attention in recent years due to their simple structure, high control accuracy, and excellent reliability [1]. They have been widely adopted in fields with stringent performance requirements such as electric vehicles, computer numerical control (CNC) machine tools, medical devices, aerospace systems, and precision instrumentation [2]. Furthermore, with the continuous advancement of modern control strategies, including Direct Torque Control (DTC) [3, 4] and Vector Control (VC) [5], the dynamic and steady-state performance of PMSMs has been significantly enhanced, offering wide speed regulation range, high precision, and smooth operation.

Despite the advantages of vector control, the conventional proportional-integral (PI) control scheme suffers from drawbacks such as integrator saturation and limited robustness against parameter variations and external disturbance [6]. These factors often degrade control performance and hinder the fulfillment of increasingly stringent industrial demands for high-precision PMSM system [7]. Moreover, under complex operational environment, PMSMs are inevitably subjected to nonlinear friction, parameter perturbation, and various uncertainties induced by temperature fluctuations and mechanical characteristics [8]. The disturbance adversely affect the steady-state behavior of stator currents and electromagnetic torque, resulting in torque ripple that compromises motion accuracy and smoothness, ultimately reducing the overall efficiency of PMSM system [9].

To achieve the precise control of a PMSM system, an improved model-free nonsingular fast terminal sliding mode control (IMFNTSMC) scheme based on a super-twisting extended sliding mode disturbance observer (STESMDO) was proposed in [10], aiming to address performance degradation and fault tolerance issues under complex operating conditions. To further mitigate the adverse effects caused by system uncertainties, Ref. [11] developed a novel sensorless nonsingular fast terminal sliding mode controller (INFTSMC), enhanced by an improved extended sliding mode disturbance observer (IESMDO). A high-order square-root cubature Kalman filter (CKF)-based adaptive estimator was integrated to enable accurate real-time estimation of motor speed and rotor position. This composite control strategy significantly improved the transient and steady-state performance of PMSMs. In [12], a new nonsingular fast terminal sliding mode surface was constructed to overcome the limitations of conventional sliding mode controllers, which often fail to ensure fast convergence under harsh external conditions. The finite-time extended state observer (FTESO) was designed to estimate system disturbances and compensate them within the speed control loop, effectively enhancing convergence speed and overall system robustness in [13].

To enhance the dynamic response speed and control accuracy of PMSM control system, this paper proposes a composite control algorithm integrating an Adaptive Non-singular Terminal Sliding Mode Control (ANTSMC) with a nonsingular fast terminal double power sliding mode observer (NFTDPSMO).

* Corresponding author: Junqin Liu (ljq2321925777@163.com).

In the composite control scheme of ANTSMC-NFTDPSMO, the ANTSMC adaptively adjusts the convergence rate based on the distance between the system state and sliding surface, thereby effectively suppressing chattering. The NFTDPSMO incorporates a coordinated design combining high-power, low-power, and linear terms, along with a denominator modification strategy, achieving singularity-free observation and global fast convergence. Simulated and experimental results demonstrate that the proposed ANTSMC-NFTDPSMO composite control method significantly mitigates the impact of parameter uncertainties, ensures finite-time convergence, and effectively improves both transient and steady-state performances while enhancing overall disturbance rejection capability.

2. MATHEMATICAL MODE OF PMSM

Under ideal conditions, the mathematical model of the PMSM in the d-q rotating reference frame can be expressed as follows [14]:

$$\begin{cases} u_d = R_s i_d + L_d \dfrac{di_d}{dt} - L_q \omega_e i_q \\ u_q = R_s i_q + L_q \dfrac{di_q}{dt} + L_d \omega_e i_d + \omega_e \psi_f \\ T_e = \dfrac{3}{2} p_n \left[\psi_f i_q + (L_d - L_q)\, i_d i_q\right] \\ T_e - T_L = \dfrac{J}{p_n}\dfrac{d\omega_e}{dt} + \dfrac{B}{p_n}\omega_e \end{cases} \tag{1}$$

where u_d and u_q are the d-axis and q-axis stator voltages, respectively; i_d and i_q are the d-axis and q-axis stator currents; L_d and L_q denote the d-axis and q-axis stator inductances; R_s is the stator phase resistance; ψ_f represents the rotor permanent magnet flux linkage; ω_e is the electrical angular velocity of the rotor; T_e is the electromagnetic torque; p_n is the number of pole pairs; T_L is the load torque; J is the moment of inertia; ω_e is the mechanical angular velocity of the rotor; and B is the damping coefficient.

In practical engineering applications, parameter variations in the PMSM are inevitable due to the influence of temperature, mechanical stress, and other environmental factors [14]. Fig. 1 shows the current component of the d-q axis of PMSM in a rotating coordinate system. Accordingly, Eq. (1) can be rewritten as:

$$\begin{cases} u_d = R_s i_d + \dfrac{d\psi_d}{dt} - \omega_e \psi_q + \Delta u_d \\ u_q = R_s i_q + \dfrac{d\psi_q}{dt} + \omega_e \psi_d + \Delta u_q \\ T_e = \frac{3}{2} n_p \left[\psi_f + (L_d - L_q) i_d\right] i_q + \Delta T_e \\ \dot{\omega}_e = \dfrac{3 n_p^2}{2J}\psi_f i_q + F \end{cases} \tag{2}$$

3. DESIGN OF ANTSMC-NFTDPSMO COMPOSITE CONTROLLER

3.1. Design of ANTSMC Controller

The speed-loop sliding mode controller is designed based on Eq. (2) as follows:

$$\dot{\omega}_e = \varepsilon i_q + F \tag{3}$$

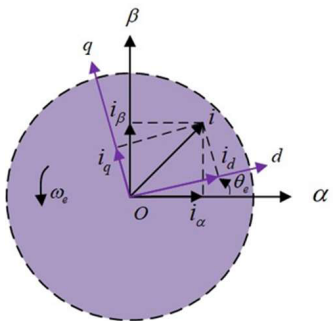

FIGURE 1. The current component of the d-q axis of PMSM in a rotating coordinate system.

where $\varepsilon = 3\,{p_n}^2\,(1/2J)\,\psi_f$ is the gain of the stator q-axis current, and F represents the system's unknown part.

Based on the equation, the speed loop sliding mode controller is designed as follows:

$$i_q^* = \frac{-F + \dot{\omega}_e^* + u}{\varepsilon} \tag{4}$$

where $\dot{\omega}_e^*$ represents the reference speed of the motor, and u denotes the control input from the feedback controller.

Letting the error between the motor's reference angular velocity and actual angular velocity be the state variable $e = \omega_e^* - \omega_e$, where$e_1 = \int e$, $e_2 = e$, and the nonsingular terminal sliding mode surface s is chosen as [17]:

$$s = e_1 + \beta e_2^a \tag{5}$$

where β is a design parameter satisfying $\beta > 0$ and $1 < a = p/q < 2$.

Taking the derivative of Eq. (5), Eq. (6) can be expressed as:

$$\dot{s} = \dot{e}_1 + \beta a e_2^{a-1}\dot{e}_2 \tag{6}$$

To balance convergence speed and chattering suppression, the following novel adaptive exponential reaching law is introduced [15]:

$$\dot{s} = \frac{-k\mathrm{sgn}\,(s)}{\lambda + (1-\lambda)\,e^{-m|s|}} - k_2 s \tag{7}$$

In this expression, $0 < \lambda < 1$, and k, λ, m, k_2 are positive constants to be designed. When $|s|$ increases, indicating that the system state is far from the sliding surface, the variable power term $-k\mathrm{sgn}\,(s)\left[\lambda + (1-\lambda)\,e^{-m|s|}\right]$ and exponential term $-k_2 s$ drive the system state toward the sliding surface. Conversely, as $|s|$ decreases, the exponential term gradually approaches zero, and the variable power term becomes dominant. Under the action of the sliding mode control law, the system state $|s|$ converges to zero, which demonstrates that as the system trajectory approaches the sliding surface, the variable-speed reaching term converges to zero gradually, thereby suppressing chattering.

By setting Eq. (6) to zero, one obtains $u_1 = \frac{e_2^{2-a}}{\beta a}$. Similarly, setting Eq. (7) to zero yields $u_2 = \frac{k\mathrm{sgn}(s)}{\lambda+(1-\lambda)e^{-m|s|}} + k_2 s$. Thus, it follows that:

$$u = u_1 + u_2 \tag{8}$$

When $k\left(\lambda+(1-\lambda)e^{-m|s|}\right)^{-1} \geq \left\|\tilde{F}\right\| + \rho(\rho>0)$, it follows that $\dot{V} \leq 0$ [18]. The detailed stability proof of ANTSMC controller is shown in Appendix A. Proof 1. The detailed proof of the stability of ANTSMC controller is shown in **Proof 1** in the appendix. Substituting Eq. (8) into Eq. (4), i_q^* is obtained as:

$$i_q^* = \frac{1}{\varepsilon}\left[\dot{\omega}_e^* + \frac{e_2^{2-a}}{\beta a} + \frac{k\mathrm{sgn}(s)}{\lambda+(1-\lambda)e^{-m|s|}} + k_2 s - F\right] \quad (9)$$

3.2. Design of NFTDPSMO Observer

Selecting the motor speed observation error as the state variable, it can be expressed as $e_b = \omega_e - \hat{\omega}_e$. Choosing the error sliding surface as $s_1 = e_b$, the sliding mode observer is designed as shown in the equation to estimate it:

$$\frac{d\hat{\omega}_e}{dt} = \varepsilon i_q + u_{smo} \quad (10)$$

where $\hat{\omega}_e$ represents the estimated speed; u_{smo} is the sliding mode control function to be designed

By subtracting Eq. (3) from Eq. (10), it can be concluded that:

$$\dot{e}_b = F - u_{smo} \quad (11)$$

The traditional dual-power reaching law exhibits slow dynamic performance, while the conventional terminal dual-power reaching law suffers from singularities and relies solely on power parameters, resulting in sluggish dynamics; both are suitable only for general control scenarios. Therefore, this section designs a non-singular fast terminal dual-power reaching law (NFTDP), as shown in Eq. (12). By introducing a denominator correction term, the NFTDP reaching law overcomes the singularity problem of traditional terminal sliding mode control, making it suitable for high-precision control systems [16].

$$\begin{aligned}\dot{s}_1 &= -\rho_1\frac{|s_1|^{\partial}\mathrm{sgn}(s_1)}{1+\delta|s_1|^{\partial-1}} - \rho_2\frac{|s_1|^{b}\mathrm{sgn}(s_1)}{1+\delta|s_1|^{b-1}} - \eta_3 s_1 \\ &= -\eta_1|s_1|^{\partial}\mathrm{sgn}(s_1) - \eta_2|s_1|^{b}\mathrm{sgn}(s_1) - \eta_3 s_1 \end{aligned} \quad (12)$$

where $\eta_1 = \frac{\rho_1}{1+\delta|s_1|^{\partial-1}}$, $\eta_2 = \frac{\rho_2}{1+\delta|s_1|^{b-1}}$, and $\delta > 0$ are used to eliminate singularities; $\partial = 1+r$, $\mathrm{b} = 1-r$, and $0 < r < 1$

According to finite-time stability theory [17], the system state will converge to $s_1 = 0$ within time $T \leq |s_1(0)|^{1-b}/[\rho_2(1-b)]$.

When $\|F\| < \eta_1|s_1|^{\partial} + \eta_2|s_1|^{b} + \eta_3\|s_1\|$ and $\dot{V}_1 \leq 0$ are satisfied, the designed observer is asymptotically stable [19]. The detailed proof of the stability of NFTDPSMO Observer is shown in **Proof 2 and Proof 3** in the appendix.

From Eq. (11) and Eq. (12), designing $u_{smo} = \eta_1|s_1|^{\partial}\mathrm{sgn}(s_1) + \eta_2|s_1|^{b}\mathrm{sgn}(s_1) + \eta_3 s_1$, $\dot{e}_b = 0$, $F = u_{smo}$. According to the sliding mode equivalent principle, $\hat{F} = \eta_1|s_1|^{\partial}\mathrm{sgn}(s_1) + \eta_2|s_1|^{b}\mathrm{sgn}(s_1) + \eta_3 s_1$. By substituting the estimated value $\hat{F}$ into Eq. (9), the designed i_q^* can be obtained as:

$$i_q^* = \frac{1}{\varepsilon}\left[\begin{array}{l}\dot{\omega}_e^* + \frac{e_2^{2-a}}{\beta a} + \frac{k\mathrm{sgn}(s)}{\lambda+(1-\lambda)e^{-m|s|}} + k_2 s \\ -\eta_1|s_1|^{\partial}\mathrm{sgn}(s_1) - \eta_2|s_1|^{b}\mathrm{sgn}(s_1) - \eta_3 s_1\end{array}\right] \quad (13)$$

The saturation function $T(s)$ [20] is adopted to replace $\mathrm{sgn}(s)$:

$$T(s) = \begin{cases} \frac{s}{\Lambda}; & |s| < \Lambda \\ \mathrm{sgn}(s); & |s| \geq \Lambda \end{cases} \quad (14)$$

where Λ denotes the boundary layer thickness. Fig. 2 illustrates the control block diagram of the system.

4. ANALYSIS OF SIMULATION RESULTS

To verify the control performance of the ANTSMC-NFTDPSMO composite controller, a simulation model is established using the MATLAB platform. The parameters of the PMSM are listed in Table 1. Table 2 shows the control parameters for three algorithms.

TABLE 1. The parameters of the PMSM.

Motor Parameters	Value
Permanent Magnet Flux Linkage ψ_f	0.171 Wb
Stator Inductance L_s	0.00334 H
Stator Resistance R_s	1.9 Ω
Pole Pairs n_p	4 pairs
Moment of Inertia J	0.001469 kg · m^2
Damping coefficient$B$	0.001 N · m · s/rad

TABLE 2. The control parameters for three algorithms.

PI	NTSMC-DPSMO	ANTSMC-NFTDPSMO
$K_p = 12$	$a_1 = 5/3$	$a = 5/3$
$K_I = 198$	$\beta_1 = 189$	$\beta = 200$
/	$k_3 = 30$	$\lambda = 0.6$
/	$k_4 = 150$	$m = 0.5$
/	$\gamma_1 = 210$	$k_2 = 210$
/	$\gamma_2 = 210$	$r = 0.6$

Remark 1: $\varepsilon = 3n_p^2\psi_e/2J$. PI parameters are tuned by Type I system and typical Type II system. In the NTSMC-DPSMO algorithm, the sliding mode surface is $s = e_1 + \beta_1 e_2^{a_1}$; the exponential convergence law is $\dot{s} = -k_3\mathrm{sgn}(s) - k_4 s$; and the DPSMO is designed to estimate the total system perturbation in real time, $\dot{s}_1 = -\gamma_1|s_1|^{l}\mathrm{sgn}(s_1) - \gamma_2 s_1$.

Remark 2: To highlight advantages of the proposed composite controller, simulations of three control methods were conducted under identical conditions in MATLAB to compare their control performances. The simulation scenarios are set as follows: at 0.2 s, ψ_f changes from 0.171 Wb to 0.150 Wb; at 0.3 s, speed n changes from 1000 r/min to 2000 r/min; at 0.5 s, θ_e

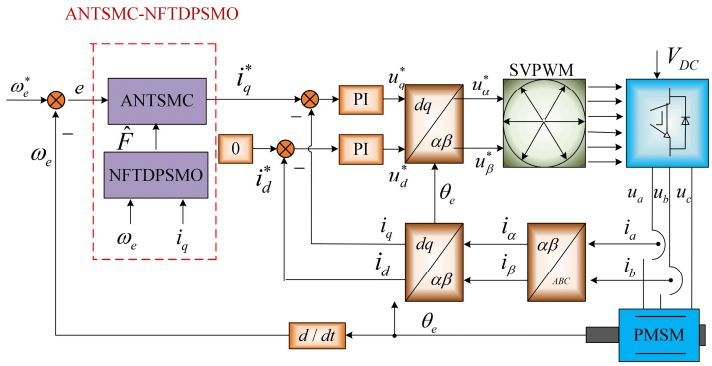

FIGURE 2. The block diagram of the PMSM system.

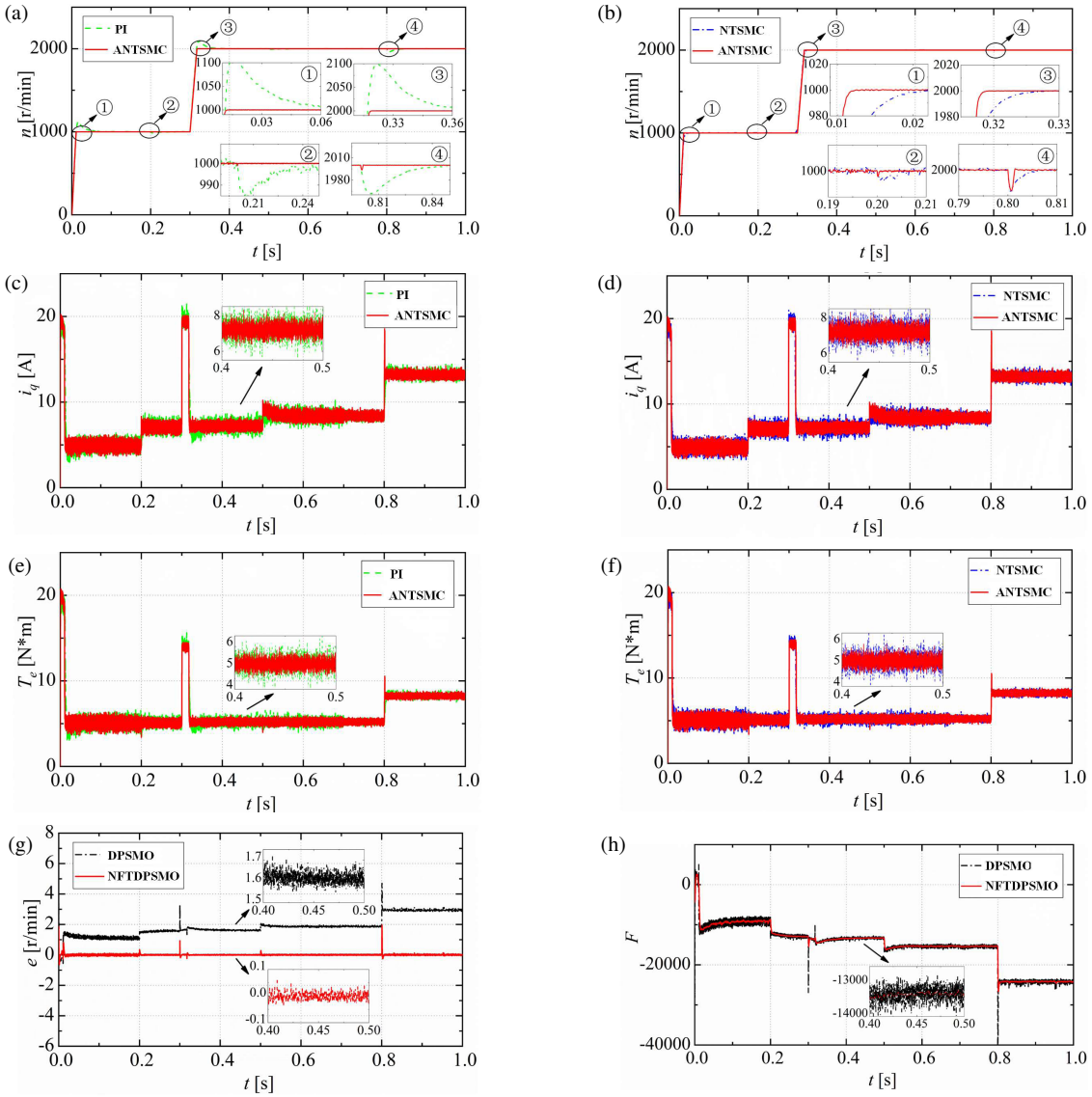

FIGURE 3. Comparative simulation results of three algorithms. (a) Simulation comparison of n for PI/ANTSMC-NFTDPSMO. (b) Simulation comparison of n for NTSMC-DPSMO/ANTSMC-NFTDPSMO. (c) Simulation comparison of i_q for PI/ANTSMC-NFTDPSMO. (d) Simulation comparison of i_q for NTSMC-DPSMO/ANTSMC-NFTDPSMO. (e) Simulation comparison of T_e for PI /ANTSMC-NFTDPSMO. (f) Simulation comparison of T_e for NTSMC-DPSMO/ANTSMC-NFTDPSMO. (g) The speed tracking error for DPSMO/NFTDPSMO. (h) The disturbance estimation $\hat{F}$ for DPSMO/NFTDPSMO.

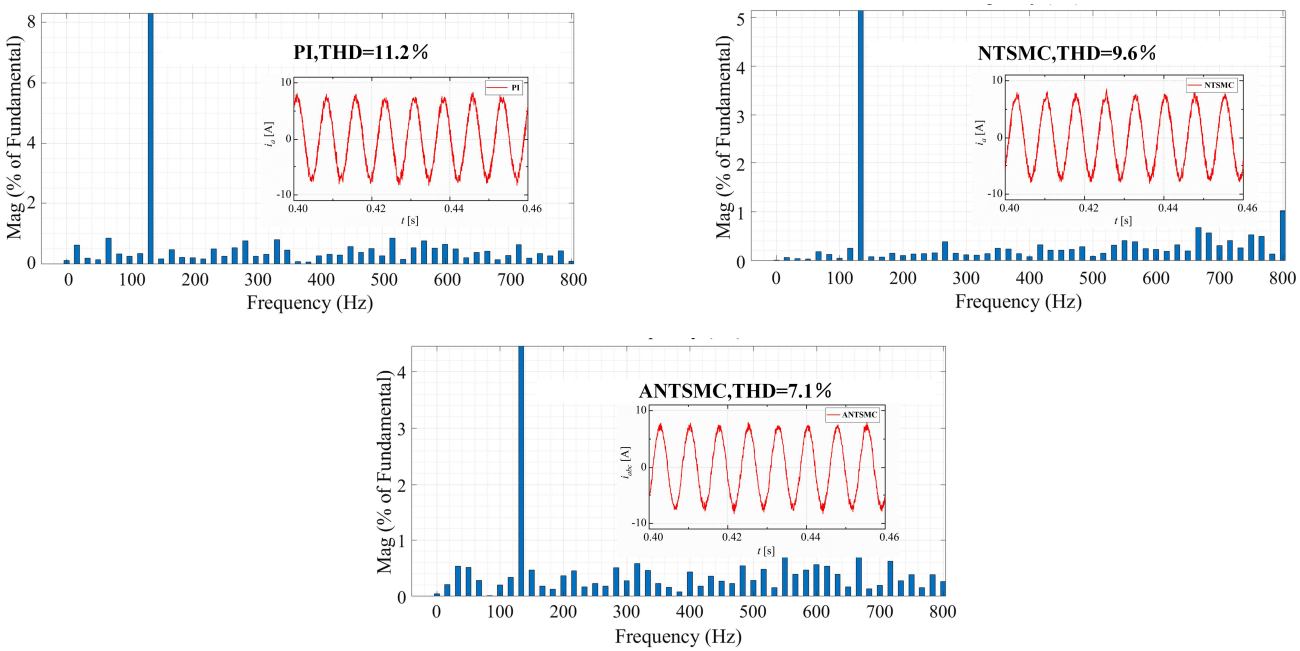

FIGURE 4. The THD analysis of Phase A stator current.

changes from 0 to $\pi/6$; at 0.6 s, resistance changes from 1.9 Ω to 3.0 Ω; at 0.7 s, stator inductance L_s changes from 0.00334 H to 0.00467 H; and at 0.8 s, load torque T_L changes from 5 N·m to 8 N·m. The simulation results are shown in Fig. 2.

The simulation results clearly illustrate the differences in control performance among the three algorithms. As shown in the speed response curves in Fig. 3(a) and Fig. 3(b), after motor startup, the PI and NTSMC-DPSMO controllers reach steady state at approximately 0.06 s and 0.03 s, respectively, whereas the ANTSMC-NFTDPSMO controller achieves steady state within 0.016 s with negligible overshoot. Under permanent magnet flux perturbations, the speed response of PI and NTSMC-DPSMO controllers is significantly affected and requires some time to recover to the desired speed, while the ANTSMC-NFTDPSMO controller promptly restores the speed to the set value. When the reference speed changes from 1000 r/min to 2000 r/min, the PI and NTSMC-DPSMO controllers take 0.06 s and 0.03 s to stabilize, respectively, whereas the ANTSMC-NFTDPSMO controller stabilizes in just 0.018 s. Furthermore, when rotor flux deviation angle, load torque, resistance, and inductance vary, the ANTSMC-NFTDPSMO method exhibits smaller speed errors and faster convergence than PI and NTSMC-DPSMO methods, demonstrating superior robustness.

As shown in Figs. 3(c)–3(f), compared to the PI and NTSMC-DPSMO methods, the ANTSMC-NFTDPSMO approach exhibits smaller current and torque ripples with smoother waveforms, which indicates that ANTSMC-NFTDPSMO method has a superior capability to suppress current and torque fluctuations, thereby effectively enhancing the performance of the PMSM control system.

In Fig. 3(g), the speed error of DPSMO fails to converge stably to zero, whereas the speed error of NFTDPSMO remains stable around zero. Both DPSMO and NFTDPSMO exhibit slight overshoot in speed error at the load change instant at 0.8 s, but overall, NFTDPSMO demonstrates superior speed tracking performance. In Fig. 3(f), both DPSMO and NFTDPSMO respond quickly to motor load variations and parameter perturbations, accurately estimating the unknown components in the control system; however, the estimated disturbance F by NFTDPSMO shows smaller oscillations than that of DPSMO, indicating better performance.

The Total Harmonic Distortion (THD) analysis of the stator current for the three methods is shown in Fig. 4. The THD of PI is 11.2%, and NTSMC-DPSMO is 9.6%, while ANTSMC-NFTDPSMO achieves a significantly lower THD of only 7.1%. In summary, compared to PI and traditional NTSMC-DPSMO, the proposed ANTSMC-NFTDPSMO composite controller can effectively reduce current harmonic distortion, suppress current and torque ripples, and enhance the system's steady-state performance. Moreover, during torque disturbances and parameter perturbations, it rapidly converges to the set point, thereby improving the system's speed tracking capability.

Table 3 summarizes the performance comparison among PI, FITSMC-STSMO, and NFITSMC-STITSMO.

TABLE 3. The comparison of the results for three algorithms.

Performances	PI	NTSMC-DPSMO	ANTSMC-NFTDPSMO
Speed Response	0.14 s	0.04s	0.02 s
Torque Ripple	16.2%	12.1%	7.1%
THD	11.2%	9.6%	7.1%
Speed Error	44 r/min	8 r/min	5 r/min

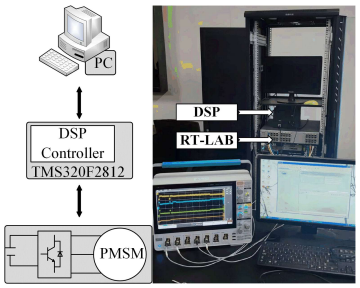

FIGURE 5. RT-LAB experimental platform.

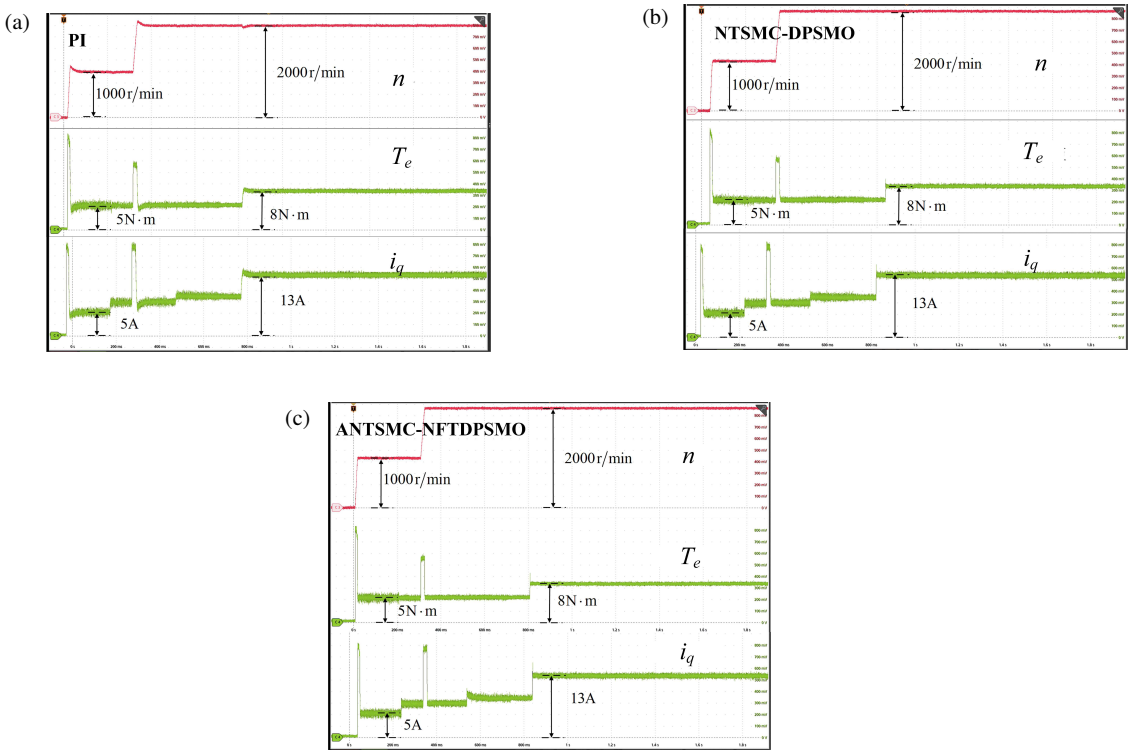

FIGURE 6. Comparison of RT-LAB experimental results. (a) Torque-Speed-Current of PI. (b) Torque-Speed-Current of NTSMC-DPSMO. (c) Torque-Speed-Current of ANTSMC-NFTDPSMO.

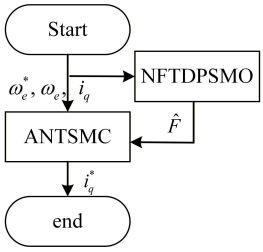

FIGURE 7. Simplified flowchart of ANTSMC-NFTDPSMO.

5. ANALYSIS OF EXPERIMENTAL RESULTS

To further validate the control performance of ANTSMC-NFTDPSMO composite controller, an RT-Lab experimental platform was established as shown in Fig. 5. The platform utilizes the TMS320F2812 DSP controller, while the PMSM drive system is simulated using an OP5600 RT-Lab real-time simulator.

Figure 6 demonstrates that under external disturbances and parameter perturbations, the ANTSMC-NFTDPSMO controller outperforms PI and NTSMC-DPSMO in terms of faster response speed and reduced current and torque ripples. This superior performance is attributed to the NFTDPSMO observer, which estimates and compensates for the system's unknown dynamics. The NFTDP reaching law within NFTDPSMO employs a synergistic design of three components (high-order term, low-order term, and linear term) along with denominator correction techniques, achieving: 1) non-singularity applicable over the entire state space; 2) global rapid convergence with optimized behavior both far from and near the sliding surface; 3) reduced chattering through smooth control signals, making it well suited for practical systems. The comprehensive performance significantly exceeds that of conventional DPSMO, demonstrating indispensable advantages in high-dynamic and high-precision control scenarios. This composite controller effectively suppresses current and torque ripples, thereby

enhancing the control accuracy of the PMSM system. Fig. 7 is a simplified flowchart of ANTSMC-NFTDPSMO.

6. CONCLUSION

To meet the increasingly demanding requirements for control precision in PMSM system, this paper proposes a compound control strategy that integrates an adaptive nonsingular terminal sliding mode control (ANTSMC) with a novel nonsingular fast terminal double-power sliding mode disturbance observer (NFTDPSMO). Comparative simulations and experiments against PI control and conventional NTSMC-DPSMO methods lead to the following conclusions. The speed loop controller, designed with an adaptive reaching law and a nonsingular terminal sliding mode surface, dynamically adjusts the convergence rate based on system states. This design effectively suppresses chattering while ensuring strong system robustness. To address the impact of external disturbances and parameter uncertainties, the proposed NFTDPSMO incorporates a triple synergistic design and a denominator modification technique. This enables singularity-free and precise estimation of system disturbances, which not only attenuates chattering but also guarantees global fast convergence. Both simulated and experimental results demonstrate that the proposed compound controller significantly enhances the disturbance rejection capability and robustness of the PMSM drive system. It achieves rapid transient response while maintaining excellent anti-interference performance.

ACKNOWLEDGEMENT

This work was supported by Postgraduate Scientific Research Innovation Project of Hunan Province Grant CX20231107.

APPENDIX A.

Proof 1: Stability Analysis of ANTSMC:

Selecting $V = \frac{1}{2}s^2$, and taking the derivative of V:

$$\begin{aligned}\dot{V}=&s\cdot\dot{s}\\ =&s\left(e_2+\beta a e_2^{a-1}\dot{e}_2\right)\\ =&s\beta a e_2^{a-1}\left(\tilde{F}-\frac{-k}{\lambda+(1-\lambda)e^{-m|s|}}\mathrm{sgn}(s)-k_2 s\right)\\ \le&\beta a e_2^{a-1}\left[\left(\left\|\tilde{F}\right\|-\frac{-k}{\lambda+(1-\lambda)e^{-m|s|}}\right)\|s\|-k_2\|s\|^2\right]\end{aligned} \tag{A1}$$

When $k\left(\lambda+(1-\lambda)e^{-m|s|}\right)^{-1}\ge\left\|\tilde{F}\right\|+\rho(\rho>0)$, it follows that $\dot{V}\le 0$ [18].

Proof 2: Stability Analysis of the NFTDPSMO:

Defining $V_1=\frac{1}{2}s_1^2$, and taking the derivative of V_1:

$$\begin{aligned}\dot{V}_1 &= s_1\dot{s}_1\\ &= s_1\left(-\rho_1\frac{|s_1|^{\partial}\mathrm{sgn}(s_1)}{1+\delta|s_1|^{\partial-1}}-\rho_2\frac{|s_1|^{b}\mathrm{sgn}(s_1)}{1+\delta|s_1|^{b-1}}-\eta_3 s_1\right)\\ &= -\rho_1\frac{|s_1|^{\partial+1}}{1+\delta|s_1|^{\partial-1}}-\rho_2\frac{|s_1|^{b+1}}{1+\delta|s_1|^{b-1}}-\eta_3 s_1^2\end{aligned} \tag{A2}$$

Since δ is very small, when $|s_1|\neq 0$, the denominator term satisfies $1+\delta|s_1|^{p-1}\approx 1(p=\partial,b)$ therefore:

$$\dot{V}_1\approx-\rho_1|s_1|^{\partial+1}-\rho_2|s_1|^{b+1}-\eta_3 s_1^2 \tag{A3}$$

Since $|s_1|^{\partial+1}=\left(s_1^2\right)^{\frac{\partial+1}{2}}$, and similarly $|s_1|^{b+1}=\left(s_1^2\right)^{\frac{b+1}{2}}$, therefore:

$$\dot{V}_1\le-\rho_2\left(2V_1\right)^{\frac{b+1}{2}}=-\rho_2 2^{\frac{b+1}{2}}V_1^{\frac{b+1}{2}} \tag{A4}$$

where $c=\rho_2 2^{\frac{b+1}{2}}$, then $\dot{V}_1\le -cV_1^{\frac{b+1}{2}}$. According to finite-time stability theory, if $\dot{V}_1\le -cV_1^{\eta}$ and $0<\eta<1$, the convergence time T satisfies $T\le\frac{V_1(0)^{1-\eta}}{c(1-\eta)}$. Solving Eq. (A5) yields:

$$T\le\frac{V_1(0)^{1-\frac{b+1}{2}}}{c\left(1-\frac{b+1}{2}\right)}=\frac{V_1(0)^{\frac{1-b}{2}}}{\rho_2\cdot 2^{\frac{b+1}{2}}\cdot\frac{1-b}{2}}=\frac{2V_1(0)^{\frac{1-b}{2}}}{\rho_2(1-b)2^{\frac{b+1}{2}}} \tag{A5}$$

Since $V_1(0)=\frac{1}{2}s_1(0)^2$, Eq. (A6) simplifies to:

$$\begin{aligned}T&\le\frac{2\left(\frac{1}{2}s_1(0)^2\right)^{\frac{1-b}{2}}}{\rho_2(1-b)2^{\frac{b+1}{2}}}=\frac{2^{\frac{b}{2}}|s_1(0)|^{1-b}}{\rho_2(1-b)2^{\frac{b+1}{2}}}\\ &\le\frac{|s_1(0)|^{1-b}}{\rho_2(1-b)}\end{aligned} \tag{A6}$$

According to finite-time stability theory [17], the system state will converge to $s_1=0$ within time $T\le\frac{|s_1(0)|^{1-b}}{\rho_2(1-b)}$.

Proof 3: Defining $V_2=1/2s_1^2$ and taking the derivative of V_2:

$$\begin{aligned}\dot{V}_2 &= s_1\dot{s}_1=e_b(F+u_{smo})\\ &= e_b(F-\eta_1|s_1|^{\partial}\mathrm{sgn}(s_1)-\eta_2|s_1|^{b}\mathrm{sgn}(s_1)-\eta_3 s_1)\\ &= e_b F-\eta_1|s_1|^{\partial}\|s_1\|-\eta_2|s_1|^{b}\|s_1\|-\eta_3\|s_1\|^2\\ &\le \|e_b\|\left(\|F\|-\eta_1|s_1|^{\partial}-\eta_2|s_1|^{b}-\eta_3\|s_1\|\right)\end{aligned} \tag{A7}$$

When $\|F\|<\eta_1|s_1|^{\partial}+\eta_2|s_1|^{b}+\eta_3\|s_1\|$ and $\dot{V}_1\le 0$ are satisfied, the designed observer is asymptotically stable [19].

REFERENCES

[1] Wang, G., D. Wang, H. Lin, J. Wang, and X. Yi, "A DC error suppression adaptive second-order backstepping observer for sensorless control of PMSM," *IEEE Transactions on Power Electronics*, Vol. 39, No. 6, 6664–6676, 2024.

[2] Liu, J., Z. Wang, F. Deng, K. Zhao, and X. Li, "Continuous high-order sliding mode optimization control of PMSM based on STSMO," *Progress In Electromagnetics Research Letters*, Vol. 127, 29–37, 2025.

[3] Zhang, Z., X. Yang, W. Wang, K. Chen, N. C. Cheung, and J. Pan, "Enhanced sliding mode control for PMSM speed drive systems using a novel adaptive sliding mode reaching law based on exponential function," *IEEE Transactions on Industrial Electronics*, Vol. 71, No. 10, 11 978–11 988, 2024.

[4] Rajeevan, P. P., *et al.*, "A direct torque control scheme with integrated commutation torque ripple reduction for BLDC motor drives with open-end windings," *IEEE Open Journal of Power Electronics*, Vol. 6, 449–463, 2025.

[5] Zhnag, Y., P. Cheng, K. Shen, W. He, D. Nian, and J. Pan, "A three-vector fast model predictive control method for steady state performance improvement," *IEEE Access*, Vol. 13, 1751–1763, 2025.

[6] Li, X., J. Liu, Y. Yin, and K. Zhao, "Improved super-twisting non-singular fast terminal sliding mode control of interior permanent magnet synchronous motor considering time-varying disturbance of the system," *IEEE Access*, Vol. 11, 17 485–17 496, 2023.

[7] Wang, F., Y. Wei, H. Young, D. Ke, H. Xie, and J. Rodríguez, "Continuous-control-set model-free predictive fundamental current control for PMSM system," *IEEE Transactions on Power Electronics*, Vol. 38, No. 5, 5928–5938, 2023.

[8] Liu, J., Y. Yang, X. Li, K. Zhao, Z. Yi, and Z. Xin, "Improved model-free continuous super-twisting non-singular fast terminal sliding mode control of IPMSM," *IEEE Access*, Vol. 11, 85 361–85 373, 2023.

[9] Dai, B., Z. Wang, J. Zhao, and S. Li, "Critical current-constrained continuous nonsingular terminal sliding mode control for PMSM based on control barrier function," *IEEE Transactions on Power Electronics*, Vol. 40, No. 10, 15 093–15 103, 2025.

[10] Li, X., J. Liu, K. Zhao, Y. Yin, and L. Zou, "An improved model-free sliding mode control algorithm of super-twisting for SPMSM," *Progress In Electromagnetics Research C*, Vol. 135, 195–210, 2023.

[11] Li, X., J. Liu, K. Zhao, Y. Yin, and L. Zou, "Improved non-singular fast terminal sensor-less sliding mode control of IPMSM considering external disturbance and parameter perturbation," *Progress In Electromagnetics Research B*, Vol. 102, 81–98, 2023.

[12] Wang, J., R. Zhou, and J. Liu, "New non-singular fast terminal sliding mode control of permanent magnet synchronous motor based on super-twisting sliding mode observer," *Progress In Electromagnetics Research C*, Vol. 146, 151–162, 2024.

[13] He, Y., K. Zhao, Z. Yi, and Y. Huang, "Improved terminal sliding mode control of PMSM dual-inertia system with acceleration feedback based on finite-time ESO," *Progress In Electromagnetics Research M*, Vol. 134, 21–30, 2025.

[14] Zhao, K., W. Liu, R. Zhou, W. Dai, S. Wu, P. Qiu, Y. Yin, N. Jia, J. Yi, and G. Huang, "Model-free fast integral terminal sliding-mode control method based on improved fast terminal sliding-mode observer for PMSM with unknown disturbances," *ISA Transactions*, Vol. 143, 572–581, 2023.

[15] Jia, N., K. Zhao, Y. Lv, and X. Li, "Non-singular fast terminal sliding mode control torsional vibration suppression for PM synchronous transmission system of EVs," *Progress In Electromagnetics Research M*, Vol. 122, 63–72, 2023.

[16] Guo, X., S. Huang, K. Lu, Y. Peng, H. Wang, and J. Yang, "A fast sliding mode speed controller for PMSM based on new compound reaching law with improved sliding mode observer," *IEEE Transactions on Transportation Electrification*, Vol. 9, No. 2, 2955–2968, 2023.

[17] Dang, C., M. Dou, S. Yan, M. Dang, Z. Hua, and D. Zhao, "A sliding mode prediction error compensation of incremental model-based deadbeat predictive current control for spmsm drives with a sliding mode speed controller," *IEEE Transactions on Transportation Electrification*, Vol. 11, No. 4, 9724–9739, 2025.

[18] Texis-Loaiza, O., J. A. Moreno, M. A. Estrada, L. Fridman, and A. Levant, "Output feedback control of nonlinear systems via lipschitz continuous sliding modes," *IEEE Control Systems Letters*, Vol. 9, 378–383, 2025.

[19] Shi, S., Y. Wang, and S. Mai, "Research on speed control of pmsm based on a new sliding mode reaching law of fast integral terminal sliding mode control with iterative-based high-gain disturbance observer," *IEEE Transactions on Industry Applications*, Vol. 61, No. 3, 4352–4363, 2025.

[20] Liu, L., H. Dong, X. Xu, Z. Tan, J. Geng, and B. Liu, "Improved sliding mode disturbance observer-based model-free finite-time terminal sliding mode control for IPMSM speed ripple minimization," *Control Engineering Practice*, Vol. 155, 106178, 2025.